ORIGINAL ARTICLE

Dynamics modeling and stability improvement in the machining of thin-walled workpiece with force-tunable pneumatic fixture

Jinjie Jia[1] · Jinbo Niu[1] · Yuwen Sun[1]

Abstract
It is very prone to cause large-amplitude cutting vibrations, or even regenerative chatter, when milling thin-walled workpiece due to its low dynamic stiffness. The utilization of fixture support is one of the most effective measures to mitigate vibrations and improve stability limits, which has gained more and more attention. However, the dynamics model of the tool-workpiece-fixture system and the influence of fixture support force have not been fully developed. In this paper, a pneumatic fixture is designed and used to exert controllable support force on the thin-walled workpiece by precisely tunning the air pressure. The position-dependent modal parameters of the thin-walled workpiece under different fixture support forces are identified by combining experimental modal test and finite element analysis. The milling dynamics is then modeled into a delay differential equation with position-dependent coefficients. On this basis, the three-dimensional stability lobe diagrams (SLDs) are obtained in the parameter space of tool path, spindle speed, and axial depth of cut. Both stable and chatter cutting tests are performed to verify the predicted SLDs, and the cutting signals under different fixture support forces are compared in detail. Experimental results reveal that the proposed model can accurately predict the chatter stability of thin-walled workpiece with fixture support, and the stability limit can be successfully improved by tunning the support force. Some important conclusions on the influence of fixture support forces are also drawn based on detailed simulation and experimental analyses.

Keywords Thin-walled workpiece · Pneumatic fixture · Support force · Dynamics modeling · Chatter stability

1 Introduction

Thin-walled workpieces are widely used in various fields such as automobile, aerospace, and energy industries [1–3].

However, due to the weak rigidity of thin-walled workpieces, it is prone to encounter regenerative chatter or large-amplitude vibrations during machining, which seriously affect the machining quality [4]. Therefore, how to improve the machining performance of thin-walled workpieces has become a major concern in both academia and industry.

Proper selection of cutting parameters via SLDs is an important way to avoid regenerative chatter [5]. Many methods have

✉ Jinbo Niu
jinboniu@dlut.edu.cn

✉ Yuwen Sun
ywsun@dlut.edu.cn

[1] Key Laboratory for Precision and Non-traditional Machining Technology of Ministry of Education, School of Mechanical Engineering, Dalian University of Technology, Dalian 116024, China

been proposed to draw SLDs in the cutting parameter space, such as the frequency domain methods [6, 7] and the time domain methods [8, 9]. Nevertheless, the prediction accuracy of SLDs for thin-walled parts is challenged by various factors. For example, the feeding movement of cutting tool and the continuous removing of material changes the dynamic properties of thin-walled workpiece. Bravo et al. [10] presented three-dimensional SLDs to incorporate the influence of tool position. Budak et al. [11] and Song et al. [12] proposed structural modification methods to simulate the effect of material removal. Eksioglu et al. [13] and Sun and Jiang [14] considered the variance of tool/workpiece dynamics along tool axis for peripheral milling of thin-walled parts. Finite element method (FEM) is widely used in the abovementioned literature to facilitate efficient simulation of time-varying and position-varying dynamics of thin-walled workpiece. But FEM cannot completely replace the experimental modal analysis (EMA) [15–17]. On the one hand, the damping ratio cannot be simulated with FEM. On the other hand, the simplification of boundary conditions may result in non-negligible prediction error of workpiece dynamics. In addition, the existence of runout [18], mode coupling [19], multiple structural modes [20], and nonlinear feedback of vibrations [21]

also affect the stability prediction accuracy. Therefore, it is not a best choice to mitigate thin-walled part milling chatter by only depending on selecting parameters from SLDs.

Low stiffness is the main reason that thin-walled workpiece suffers from regenerative chatter and large-amplitude forced vibrations. Using fixture support to enhance the dynamic stiffness of thin-walled workpiece could essentially improve the cutting performance of thin-walled workpieces. Kolluru et al. [22] reported that the utilization of ancillary fixture could reduce the milling vibrations to one-eighth of the original level during the milling process of thin-walled casing. Ma et al. [23] found that magnetorheological fluid flexible fixture could significantly improve the stability limit of thin-walled workpiece. Fei et al. [24] discovered that the milling deformation could be effectively suppressed by placing a moving fixture element on the uncut surface of thin-walled workpiece.

In order to investigate the mechanism of vibration suppression and stability improvement of fixture on thin-walled workpiece, analytical methods and finite element methods are successively used to model the dynamics of fixture-workpiece system. Based on Rayleigh-Ritz method, Meshreki et al. [25] proposed an analytical formulation to represent the dynamic responses of multipocket thin-walled structures under fixture constraints, and further built multispan beam models to account for the effect of material removing [26]. Finite element simulation verified that the predicted error is less than 5%. Wan et al. [27, 28] regarded the fixture-workpiece system as an equivalent thin-multi-span plate with intermediate line and point supports, and set up the dynamic equation using the Lagrangian method. The aforementioned methods and simulation results provide reference for fixture design and tunning.

It is worth noting that simple utilization of fixture cannot always improve machining performance. The workpiece position error, fixture-induced deformation error, and datum error may damage the machining precision [29–31]. It is a prerequisite to figure out the influences of fixture design parameters and tunning schemes. Liu et al. [32] optimized the number and positions of locators on the secondary locating surface, which guaranteed the machining precision with minimum locators. Raghu and Melkote [33] analyzed the influence of clamping sequence on workpiece position and orientation. Siebenaler and Melkote [34] studied the role of compliance of the fixture body on workpiece deformation using finite element method. Wan et al. [28] investigated the influence of fixture layout on dynamic response of thin-walled multiframed workpiece. On this basis, the layout was further optimized by Wan and Zhang [27] to improve the machining stability. Matsubara et al. [35] reported that fixture support with surface contact performed better than point contact at suppressing machining vibrations. Zhong and Hu [36] proposed N-2-1 fixturing scheme to mitigate machining deformation for large-scale thin-walled workpiece. Hao et al. proposed 6+X locating principle [37] and machining sequence adaptive tunning scheme [38] to control milling deformation.

Nevertheless, to the best of the authors' knowledge, few studies concentrate on the quantitative influences of support force on milling dynamics of thin-walled workpiece, partially due to the lack of controllable actuators. This paper proposes an effective method to model the tool-workpiece-fixture system dynamics and studies the influences of different support forces, where the precise control of support force is realized through an innovative design of pheumatic fixture, as shown in Fig. 1. The
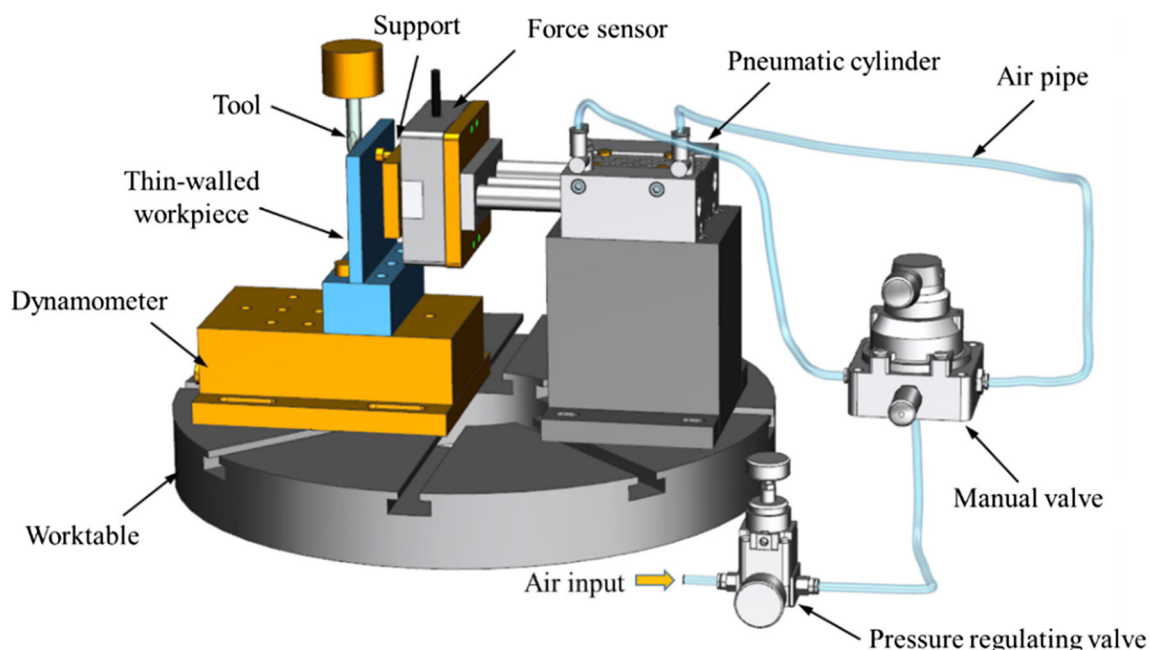

Fig. 1 Workpiece-fixture system with precise control of support force

remainder of this paper is organized as follows. Section 2 establishes the dynamic model of the system. Section 3 calculates the stability of the system. Section 4 carries out the experimental verification. Section 5 concludes the paper.

2 Dynamic model of the system

2.1 Dynamic equation of the tool-workpiece-fixture system

The schematic diagram of tool-workpiece-fixture system is shown in Fig. 1, where the pneumatic fixture support locates at the uncut side of the thin-walled workpiece and the support force can be precisely controlled via the pneumatic cylinder. The dynamic equation of the system can be expressed in physical space as:

$$M_{wf}\ddot{q}(t) + C_{wf}\dot{q}(t) + K_{wf}q(t) = F(t) \tag{1}$$

where $\mathbf{M}_{wf}$, $\mathbf{C}_{wf}$, $\mathbf{K}_{wf}$ are the mass, damping, and stiffness matrices, respectively; $\ddot{\mathbf{q}}(t)$, $\dot{\mathbf{q}}(t)$, and $\mathbf{q}(t)$ are the acceleration, velocity, and displacement, respectively; $\mathbf{F}(t)$ is the cutting force vector.

The dynamic equation can be transformed from physical space to modal space by [39]:

$$\mathbf{q}(t) = \mathbf{P}\boldsymbol{\Gamma}(t) \tag{2}$$

where $\mathbf{P}$ is the mode shape matrix, and $\boldsymbol{\Gamma}(t)$ is the modal displacement vector.

$$P = \begin{bmatrix} P_T & -P_{Wf} \end{bmatrix}$$

$$= \begin{bmatrix} p_{1x,1;T} & \cdots & p_{1x,m_T;T} & -p_{1x,1;Wf} & \cdots & -p_{1x,m_{Wf};Wf} \\ p_{1y,1;T} & \cdots & p_{1y,m_T;T} & -p_{1y,1;Wf} & \cdots & -p_{1y,m_{Wf};Wf} \\ \vdots & \ddots & \vdots & \vdots & \vdots & \vdots \\ p_{nx,1;T} & \cdots & p_{nx,m_T;T} & -p_{nx,1;Wf} & \cdots & -p_{nx,m_{Wf};Wf} \\ p_{ny,1;T} & \cdots & p_{ny,m_T;T} & -p_{ny,1;Wf} & \cdots & -p_{ny,m_{Wf};Wf} \end{bmatrix}_{2n \times (m_T + m_{Wf})},$$

$$\Gamma(t) = \begin{bmatrix} \Gamma_{1;T} \\ \vdots \\ \Gamma_{m_T;T} \\ \Gamma_{1;Wf} \\ \vdots \\ \Gamma_{m_{Wf};Wf} \end{bmatrix}_{(m_T + m_{Wf}) \times 1}$$

$$\tag{3}$$

where n is the number of contact points between tool and workpiece; m_T and m_{Wf} represent the number of modes for the tool and the workpiece-fixture subsystem, respectively; $\mathbf{P}_T$ and $\mathbf{P}_{Wf}$ are the mode shape submatrices with regard to the tool and the workpiece-fixture, respectively; the element $p_{AB,C;D}$ in matrix $\mathbf{P}$ denotes the mode shape value, where the

subscripts mean $A = 1 \cdots n$ is the serial number of discrete contact node between tool and workpiece, $B = x$ or y is the direction of vibrations, $C = 1 \cdots m_T$ or $1 \cdots m_{Wf}$ is the serial number of mode for the tool or the workpiece-fixture, and $D = m_T$ or m_{Wf} represents the tool or the workpiece-fixture; The element $\Gamma_{E;F}$ in matrix $\boldsymbol{\Gamma}(t)$ denotes the modal displacement, where the subscripts mean $E = 1 \cdots m_T$ or $1 \cdots m_{Wf}$ is the serial number of mode for the tool or the workpiece-fixture, and $F = m_T$ or m_{Wf} represents the tool or the workpiece-fixture.

Substituting Eq. (2) into Eq. (1), the dynamics equation in modal space can be written as:

$$M_\Gamma \ddot{\Gamma}(t) + C_\Gamma \dot{\Gamma}(t) + K_\Gamma \Gamma(t) = P^T F(t) \tag{4}$$

where $\mathbf{M}_\Gamma$, $\mathbf{C}_\Gamma$, $\mathbf{K}_\Gamma$ are the modal mass, modal damping, and modal stiffness matrices, respectively:

$$\begin{aligned} M_\Gamma &= \mathrm{diag}\big(m_{1;T}, \cdots, m_{m_T;T}, m_{1;Wf}, \cdots, m_{m_{Wf};Wf}\big), \\ C_\Gamma &= \mathrm{diag}\big(c_{1;T}, \cdots, c_{m_T;T}, c_{1;Wf}, \cdots, c_{m_{Wf};Wf}\big), \\ K_\Gamma &= \mathrm{diag}\big(k_{1;T}, \cdots, k_{m_T;T}, k_{1;Wf}, \cdots, k_{m_{Wf};Wf}\big), \end{aligned} \tag{5}$$

where $m_{a;\,T}$, $c_{a;\,T}$, $k_{a;\,T}(a = 1, 2, \cdots, m_T)$ are the modal mass, modal damping, and modal stiffness with regard to the a-th mode of the tool, respectively; $m_{b;\,Wf}$, $c_{b;\,Wf}$, $k_{b;\,Wf}(b = 1, 2, \cdots, m_{Wf})$ are the modal mass, modal damping, and modal stiffness with regard to the b-th mode of the workpiece-fixture subsystem, respectively. The modal parameters in Eq. (5) are obtained by combining EMA and FEM in this paper, which will be detailed in Section 2.3.

2.2 Cutting force modeling considering runout

As shown in Fig. 2, the inevitable tool runout phenomenon changes the equivalent cutting radius, causes multiple regeneration, affects the stability limits, and thus should be taken into account in dynamics modeling [40]. Based on the mechanistic force model [5], the elemental cutting forces in tangential and radial directions can be expressed as:

$$\begin{bmatrix} dF_t(t,j,k) \\ dF_n(t,j,k) \end{bmatrix} = g(\varphi(t,j,k)) \left\{ \begin{bmatrix} k_{tc} \\ k_{nc} \end{bmatrix} h(t,j,k)dz + \begin{bmatrix} k_{te} \\ k_{ne} \end{bmatrix} ds \right\} \tag{6}$$

where k_{tc} and k_{nc} are the shear force coefficients in tangential and radial directions, respectively; k_{te} and k_{ne} are the edge force coefficients in tangential and radial directions, respectively; dz and ds are the axial height and edge length with regard to each discrete slice, respectively; $\varphi(t,j,k)$ and $h(t,j,k)$ are the instantaneous rotation angle and the instantaneous uncut chip thickness with regard to cutting element (j, k) at time t, respectively; and $g(\varphi(t,j,k))$ is an unit step function to determine whether the element is cutting or not:
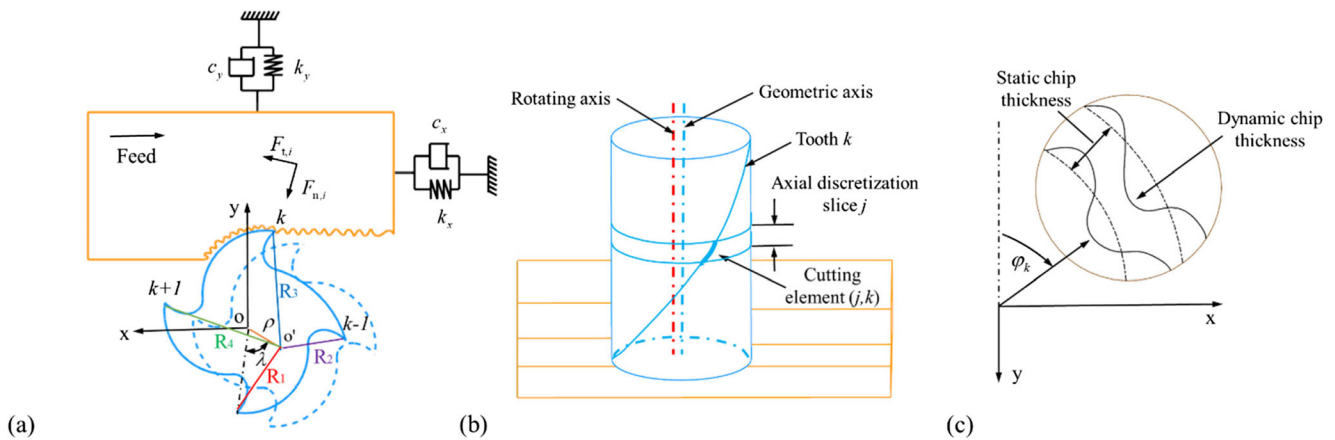
Fig. 2 Schematic diagram of the milling process. **a** 2-DOF milling considering runout. **b** Discretization of the helix tool. **c** Dynamic chip thickness

$$g(\varphi(t,j,k))$$
$$= \begin{cases} 1, & \varphi_{st}(j,k) \leq \mathrm{mod}(\varphi(t,j,k), 2\pi) \leq \varphi_{ex}(j,k) \\ 0, & \text{otherwise} \end{cases} \quad (7)$$

where $\varphi_{st}(j,k)$ and $\varphi_{ex}(j,k)$ are the start and exit angles, respectively.

The instantaneous rotation angle $\varphi(t,j,k)$ is:

$$\varphi(t,j,k) = \frac{2\pi\Omega}{60}t - \frac{z_j\tan(\beta_k)}{R} + \varphi_{ref} \quad (8)$$

where Ω is the spindle speed in revolution per minute, z_j is the axial height of the j-th slice, β_k is the helix angle of Tooth k, R is the radius of the tool, and φ_{ref} is the angular distance between Tooth k and negative y axis at the tool tip at $t = 0$.

Due to the effects of chip regeneration, the instantaneous uncut chip thickness in Eq. (6) contains two parts: the quasi-static part $h_s(t,j,k,p)$ and the dynamic part $h_d(t,j,k,p)$.

$$h(t,j,k,p) = h_s(t,j,k,p) + h_d(t,j,k,p) \quad (9)$$

where

$$h_s(t,j,k,p) = f_t(t,j,k:k-p)\sin\varphi(t,j,k)$$
$$+ R(j,k) - R(j,k-p) \quad (10)$$

and

$$h_d(t,j,k,p) = [x(t) - x(t-\tau(j,k,p))]\sin\varphi(t,j,k) - [y(t) - y(t-\tau(j,k,p))]\cos\varphi(t,j,k) \quad (11)$$

where p denotes the runout induced multi-regenerative index; $f_t(t,j,k:k-p)$ is the feed between Tooth k and Tooth $k-p$ at the j-th axial slice; $\tau(j,k,p)$ denotes the multi-regenerative time delay; $R(j,k)$ and $R(j,k-p)$ are the actual rotating radius of Tooth k and Tooth $k-p$, respectively.

$$R(j,k) = \sqrt{R^2 + \rho^2 - 2R\rho\cos(\theta_t)} \quad (12)$$

where

$$\theta_t = \min\left\{\lambda - \psi(j,k:1) - z_j\frac{\tan(\beta_k)}{R}\right\} \quad (13)$$

where ρ is the runout offset and λ is the runout orientation; $\psi(j,k:1)$ is the pitch angle between Tooth k and Tooth 1 on axial height z_j.

The multi-regenerative instantaneous uncut chip thickness $h(t,j,k,p)$ can be calculated efficiently by:

$$h(t,j,k,p) = \max\{\min[h(t,j,k,p), p = 1, \cdots, N], 0\} \quad (14)$$

where N denotes the number of teeth.

Once the instantaneous uncut chip thickness and cutting force coefficients are obtained, the cutting forces for each element can be expressed in Cartesian coordinate system as:

$$\begin{bmatrix} dF_x(t,j,k) \\ dF_y(t,j,k) \end{bmatrix} = \begin{bmatrix} -\cos\varphi(t,j,k) & -\sin\varphi(t,j,k) \\ -\sin\varphi(t,j,k) & \cos\varphi(t,j,k) \end{bmatrix} \begin{bmatrix} dF_t(t,j,k) \\ dF_n(t,j,k) \end{bmatrix} \quad (15)$$

Finally, the total instantaneous cutting forces are:

$$\begin{bmatrix} F_x(t) \\ F_y(t) \end{bmatrix} = \sum_{j=1}^{N_a}\sum_{k=1}^{N} \begin{bmatrix} dF_x(t,j,k) \\ dF_y(t,j,k) \end{bmatrix} \quad (16)$$

where N_a is the number of discrete axial slices.

2.3 Identification of dynamic parameters

The dynamic parameters of thin-walled workpiece change with the movement of cutting point. Fixture support further complicates the identification of position-dependent frequency response function (FRF). In this subsection, FRF of the
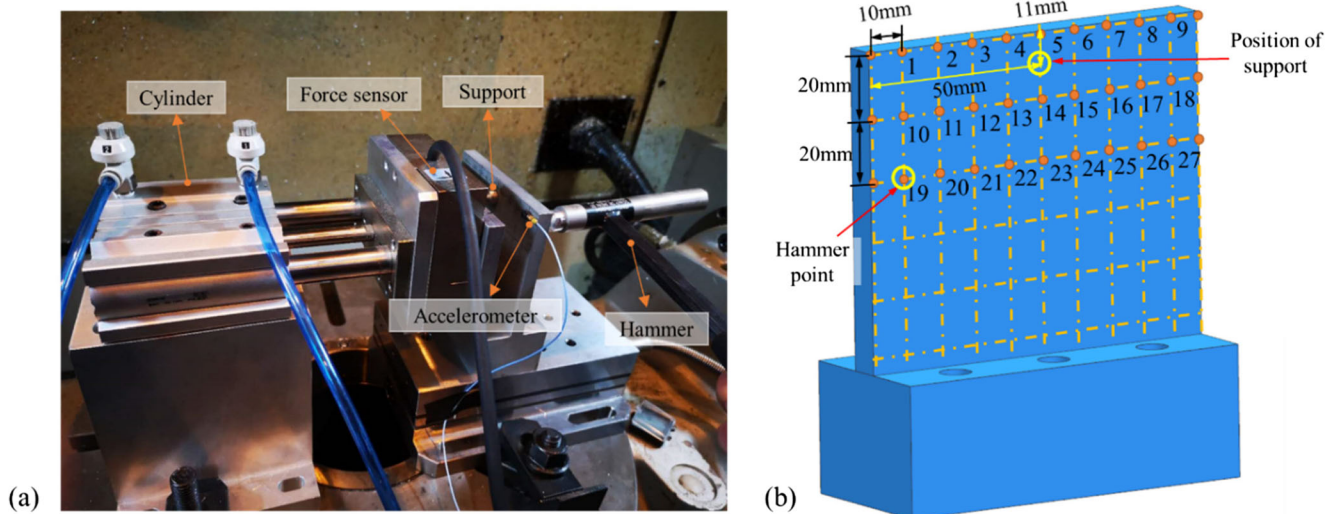
Fig. 3 Experimental modal test. **a** Setup. **b** Thin-walled workpiece

workpiece-fixture subsystem is identified by combining EMA and FEM, i.e., the modal parameters are identified using EMA and the mode shapes are simulated using FEM.

Step 1: Modal parameter identification using EMA

Modal parameters including natural frequencies and damping ratios are identified using experimental modal tests, as shown in Fig. 3. An impact hammer (PCB 086C01) is used to excite the thin-walled plate (aluminum alloy 7075, 100mm × 9mm × 85mm) and a miniature accelerometer (352C23) is used to measure the dynamic responses at each discrete node. Since it is very prone to encounter double-hit during the hammer test of thin-walled workpiece, the driving point (i.e., point where hammer excitation and response reception locate at the same position) is chosen far away from the plate corner (i.e., position with the lowest stiffness), as shown in Fig. 3 b. By moving the accelerometer from Point 1 to Point 27, the mode shapes are also experimentally identified, which will be used to validate the simulation results of FEM in the next section.

The end of fixture support is a cylindrical rod (aluminum alloy 7075) with 5mm diameter. Since the workpiece in Fig. 3 b has multiple modes, the mode coupling effect will

consequently make the analysis very complicated. In order to better understand the influence of fixture support, the support position is placed at the middle of the workpiece, i.e., the node of the torsional mode shape, as shown in Fig. 3 b.

Modal tests are performed for different supporting conditions. For the case without support, the cylindrical rod is out of contact with the plate surface. For the case with support, the cylindrical rod is in contact with the uncut surface of the plate, and the support force is tuned with the air pressure regulating valve and measured with the force sensor (Fig. 1). In this paper, 0N, 40N, 60N, 80N, 100N, and 120N are chosen for comparison study. 0N means that the cylindrical rod is in contact with the plate but the support force is 0N (the air pressure is 0Pa).

Take 80N as an example. The FRFs with and without fixture support are compared in Fig. 4. It reveals that the fixture support exerts considerable influence on the dynamic properties of thin-walled workpiece, in terms of natural frequency and FRF amplitude. The first mode shifts to higher frequency band and splits into two modes. Meanwhile, the FRF amplitude reduces from 3.84×10^{-3} mm/N to 2.00×10^{-4} mm/N and 1.85×10^{-4} mm/N, as shown in Fig. 4 b. For the second mode, since the support
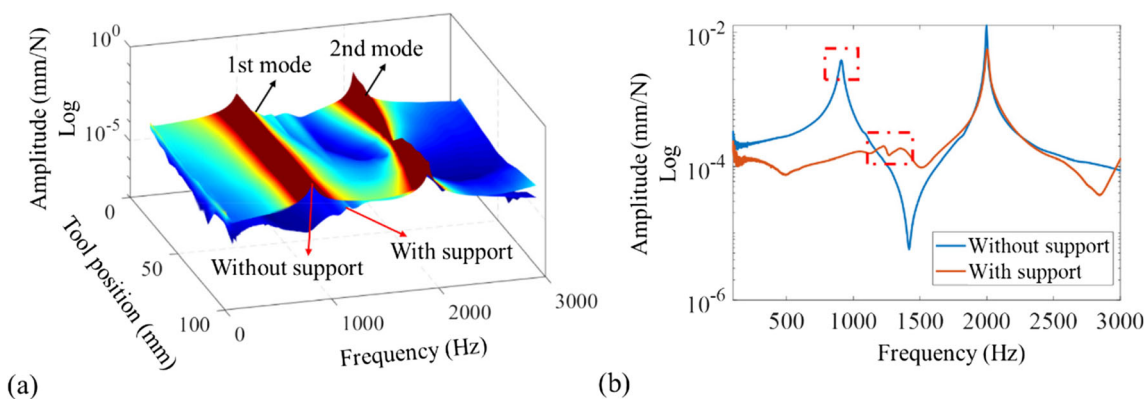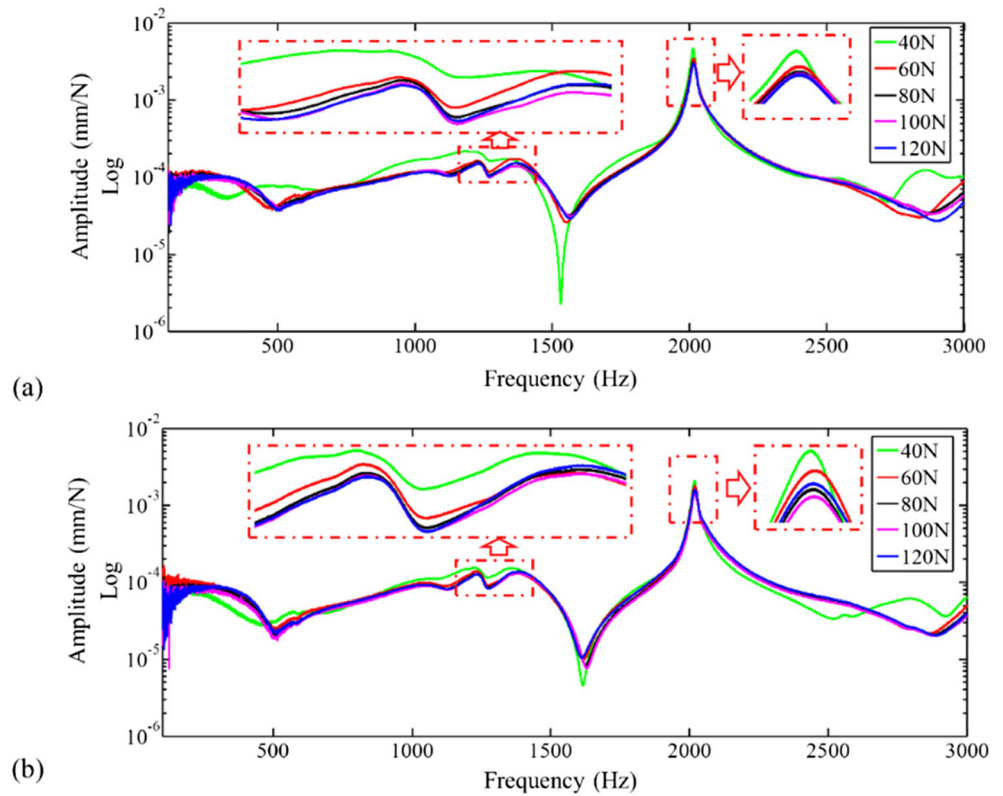

Fig. 4 Comparisons of measured FRFs for cases with and without fixture support. **a** Comparisons at different tool position. **b** Comparisons at Point 1

Fig. 5 Comparisons of FRFs under different support forces. **a** FRFs at Point 3. **b** FRFs at Point 4

(a)

(b)

rod locates at the node of mode shape, the natural frequency does not change and the amplitude is slightly reduced.

The influence of support force on FRF of thin-walled workpiece is illustrated in Fig. 5. Generally speaking, the change of support force has almost no effect on the natural frequency of each mode, while the FRF amplitude slightly decreases as the growth of support force. Nevertheless, when the support force reaches to a certain value, the variance of FRF amplitude becomes negligible. For example, the FRF

curves with regard to 80N, 100N, and 120N are almost the same, as shown in Fig. 5 b. This may attribute to the reason that when support force is small, the contact status between workpiece and support is not stable. Enough preload (the critical values is around 80N in this case) is necessary for the workpiece-fixture subsystem to exert stable FRF.

Based on the above analysis, FRFs when the contact status between workpiece and fixture is stable are used for modal parameter identification with the least squares complex
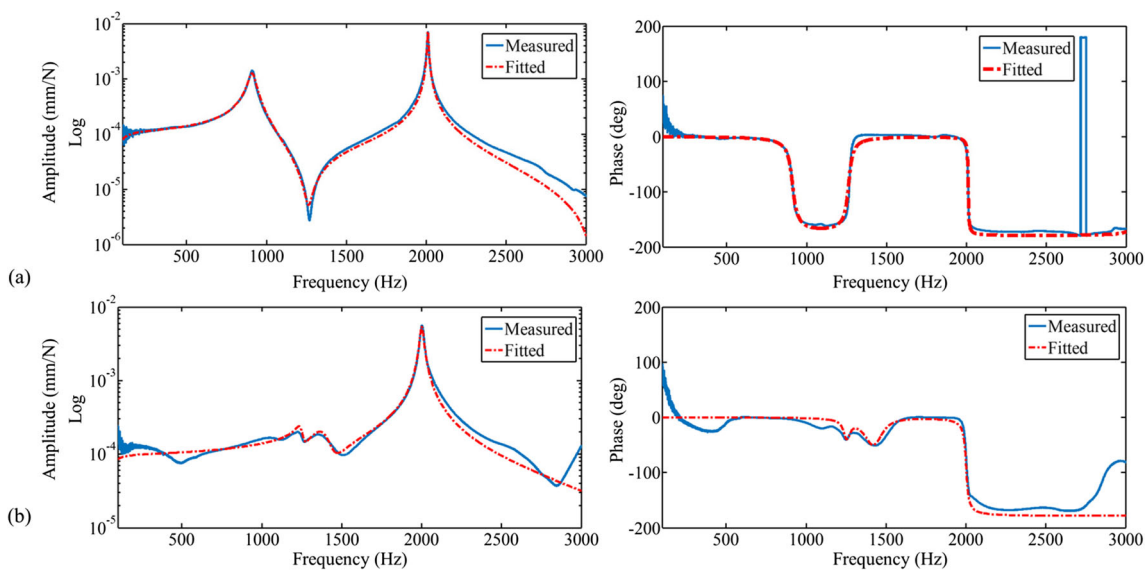

Fig. 6 Measured and fitted FRFs of the workpiece. **a** Without support. **b** With support

Table 1 Identified modal parameters for workpiece with and without support

Condition	Mode no.	Natural frequency (Hz)	Damping ratio (%)	Modal mass (kg)
Without support	1	920.2	3.72	0.4016
	2	2012.4	0.17	0.2575
With support	1	1225.3	5.18	2.8062
	2	1379.3	4.37	3.2203
	3	2016.9	0.29	0.2543

frequency (LSCF) method embedded in LMS Test Lab software. The measured and fitted FRF curves are shown in Fig. 6 and the identified modal parameters are listed in Table 1 for workpiece with and without fixture support, respectively. The support force is 80N in this case.

Step 2: Mode shape extraction using FEM

The utilization of FEM can significantly reduce the burden of experimental modal test, especially for mode shape identification of thin-walled workpiece. In this paper, the commercial software ABAQUS is used to predict the natural frequencies and mode shapes of the thin-walled plate with fixture support. The material properties are set to density $\rho_d = 2800 \text{kg/m}^3$, elastic modulus $E = 71 \text{Gpa}$, and Poisson's ratio $\upsilon = 0.33$ for aluminum alloy 7075. In the simulation, the bottom of the workpiece is fixed. The fixture support is simulated by using preloading condition with the following contact options: friction in the tangential direction is set to rough, and hard contact is used in the normal direction and set to allow separation after contact. For the interaction options, the finite slip formula and the surface-surface discretization method are used. For the support boundary options, the tangential direction
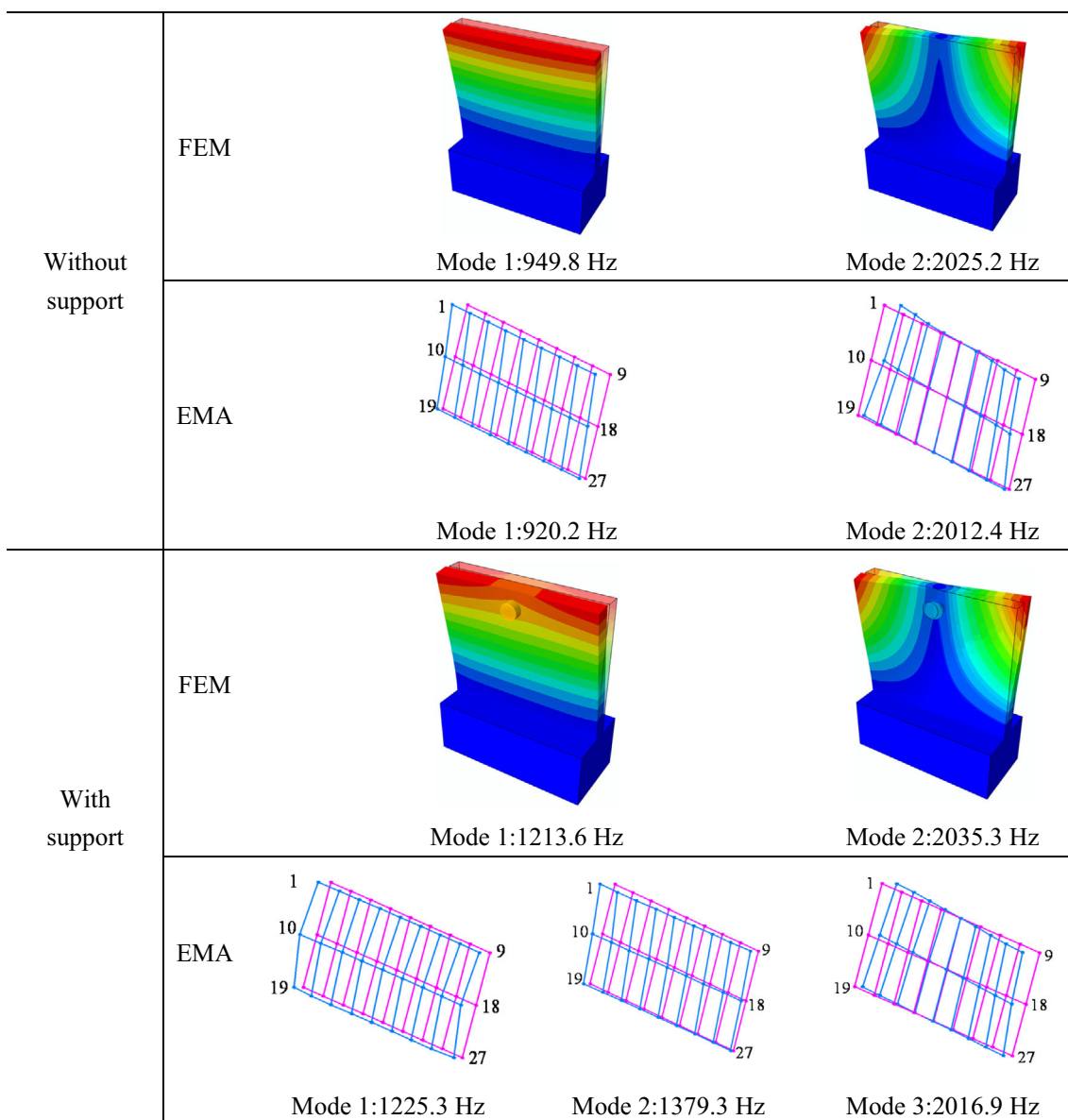

Fig. 7 Comparisons of FEM and EMA in terms of natural frequency and mode shape

is restricted and the normal direction is free. The FEM outputs for workpieces with and without fixture support are shown in Fig. 7.

According to Fig. 7, the simulation results of FEM are in good agreement with the experimental results of EMA for the case without fixture support, in terms of both natural frequencies and mode shapes. It indicates that the boundary conditions and material inputs of FEM are acceptable. For the case with fixture support, the natural frequency and mode shape of the second mode still match well. However, the FEM only output one bending mode at 1213.6Hz, while the EMA shows two bending modes at 1225.3Hz and 1379.3Hz, respectively. This discrepancy may attribute to the very complicated nonlinear interaction at the contact position after the fixture support is added, and specific in-depth analysis needs to be further explored. In this paper, the advantages of FEM and EMA are combined, i.e., the modal parameters including natural frequencies, damping ratios, and normalized mode shape values at driving point are identified using EMA, and the mode shapes are extracted using FEM. Two bending modes and one torsional mode for cases with support are used to predict the 3D SLDs in Section 3.

Step 3: Identification of dynamic parameters at each point on the cutting path

Natural frequencies and mode shapes are inherent properties of structure, and thus do not change with cutting position. The change of dynamics along tool path is represented by the mode shape values. In Step 1, the mode shape value is normalized at driving point, i.e., the mode shape value at driving point is 1. Take the same normalization rule on the extracted

mode shapes in Step 2, i.e., all values are divided by the shape value at the same driving point, which produces the resultant mode shape values for all discrete points on the cutting path.

3 Stability calculation

According to Section 2, the governing dynamic equation can be re-organized as:

$$M_\Gamma \ddot{\Gamma}(t) + C_\Gamma \dot{\Gamma}(t) + K_\Gamma \Gamma(t)$$
$$= \sum_{k=1}^{N} \sum_{j=1}^{N_a} \left\{ P^T K_c(t,j,k) P[\Gamma(t) - \Gamma(t - \tau(j,k))] \right\}$$
$$+ \sum_{k=1}^{N} \sum_{j=1}^{N_a} P^T F_0(t,j,k) \qquad (17)$$

where

$$K_c(t,j,k) = \mathrm{diag}(\, 0_{4\times4} \quad \cdots \quad 0_{4\times4} \quad K_{c,ele}(t,j,k) \quad 0_{4\times4} \quad \cdots \quad 0_{4\times4} \,),$$

$$F_0(t,j,k) = \mathrm{diag}(\, 0_{2\times1} \quad \cdots \quad 0_{2\times1} \quad F_{0,ele}(t,j,k) \quad 0_{2\times1} \quad \cdots \quad 0_{2\times1} \,) \qquad (18)$$

where $\mathbf{K}_{c,\,ele}(t,j,k)$ is the directional coefficient matrix, and $\mathbf{F}_{0,\,ele}(t,j,k)$ is the cutting force matrix.

$$K_{c,ele}(t,j,k) = g(\varphi(t,j,k)) \begin{bmatrix} -\cos\varphi(t,j,k) & -\sin\varphi(t,j,k) \\ -\sin\varphi(t,j,k) & \cos\varphi(t,j,k) \end{bmatrix} \begin{bmatrix} k_{tc} \\ k_{nc} \end{bmatrix} [\sin\varphi(t,j,k) \quad -\cos\varphi(t,j,k)] dz$$

$$F_{0,ele}(t,j,k) = g(\varphi(t,j,k)) \begin{bmatrix} \cos\varphi(t,j,k) & \sin\varphi(t,j,k) \\ -\sin\varphi(t,j,k) & \cos\varphi(t,j,k) \end{bmatrix} \left(\begin{bmatrix} k_{tc} \\ k_{nc} \end{bmatrix} h_s(t,j,k) dz + \begin{bmatrix} k_{te} \\ k_{ne} \end{bmatrix} ds \right) \qquad (19)$$

To predict the stability of the system, Eq. (17) can be transformed from modal space into state space:

$$\dot{x}(t) = Ax(t)$$
$$+ \sum_{k=1}^{N} \sum_{j=1}^{N_a} \left\{ B(t,j,k)[x(t) - x(t - \tau(j,k))] + D(t,j,k) \right\} \qquad (20)$$

where

$$x(t) = \begin{bmatrix} \Gamma(t) \\ \dot{\Gamma} \end{bmatrix}(t), A = \begin{bmatrix} 0 & I \\ -M_\Gamma^{-1} K_\Gamma & -M_\Gamma^{-1} C_\Gamma \end{bmatrix},$$
$$B(t,j,k) = \begin{bmatrix} 0 & 0 \\ M_\Gamma^{-1} P^T K_c(t,j,k) P & 0 \end{bmatrix}, \qquad (21)$$
$$D(t,j,k) = \begin{bmatrix} 0 \\ M_\Gamma^{-1} P^T F_0(t,j,k) \end{bmatrix}$$

On the basis of Eq. (20), the multi-regenerative stability can be analyzed by using the Floquet theory. In this paper, the

proposed method in Ref. [41] is expanded to predict the stability of thin-walled workpiece with tool runout under fixture support constraints.

4 Experimental verification

In this section, the 3D SLDs of the thin-walled plate with and without support are predicted and verified through experiments. In addition, a series of comparisons and analyses are

Table 2 Identified cutting force coefficients and runout parameters.

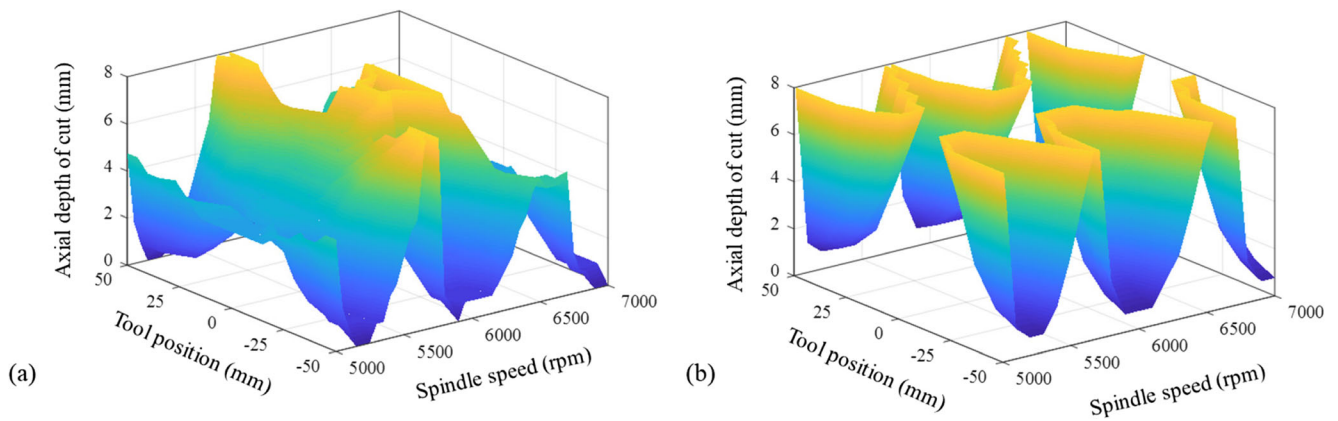| K_{tc} (N/mm²)	K_{te} (N/mm)	K_{nc} (N/mm²)	K_{ne} (N/mm)	ρ (μm)	λ (deg.)
957.41	25.84	298.14	19.26	2.8	330

Fig. 8 Three-dimensional stability lobe diagrams. **a** Without support. **b** With support

carried out on the cutting process under different support forces.

4.1 Cutting tests of workpiece with and without support

Prior to stability analysis, the cutting force coefficients and runout values are obtained based on the methods proposed in Ref. [42]. In this paper, a three-flute solid carbide end mills with diameter 20 mm and helix angle 45° is used to perform all the cutting tests. The identified parameters are listed in Table 2.

Considering the position dependency of system dynamics, the stability limits are drawn in a three-dimensional parameter space composed of spindle speed, tool position, and axial depth of cut. Both the cases with and without fixture support are demonstrated, as shown in Fig. 8 a and b. Figure 8 reveals that there is indeed an improvement in the stability limit after adding fixture support.

The experimental setup is shown in Fig. 9. The thin-walled workpiece (aluminum alloy 7075) is fixed to Kistler dynamometer (9257B) by using six bolts. During the milling process, two miniature accelerometers (PCB 352C23 with sensitivity 5.33mV/g and 5.53 mV/g, respectively) are fixed on the uncut side of the workpiece to record acceleration signals in the direction of thickness, and a microphone (GRAS 46AE with sensitivity 50 mV/Pa) is also used to collect sound pressure.

Since this paper mainly studies the influence of support force on the dynamics of thin-walled workpiece, how to accurately control the support force is very important. Here, a pneumatic cylinder is introduced into the experimental design to ensure constant support force, which is controlled by the air pressure regulating valve as marked by the red circle in Fig. 9. In addition, to read the magnitude of support force, a force sensor is installed between the fixture support and the output end of the pneumatic cylinder.

To further verify the prediction results, a series of experiments are carried out. The axial depth of cut is kept constant along the whole tool path ($a_p = 3$mm). Therefore, the predicted 3D SLDs in Fig. 8 can be interpreted by a sectional view, as shown in Fig. 10 a for case without support and Fig. 10 e for case with support, where the colored area represents chatter zone and the uncolored area represents stable zone. The radial
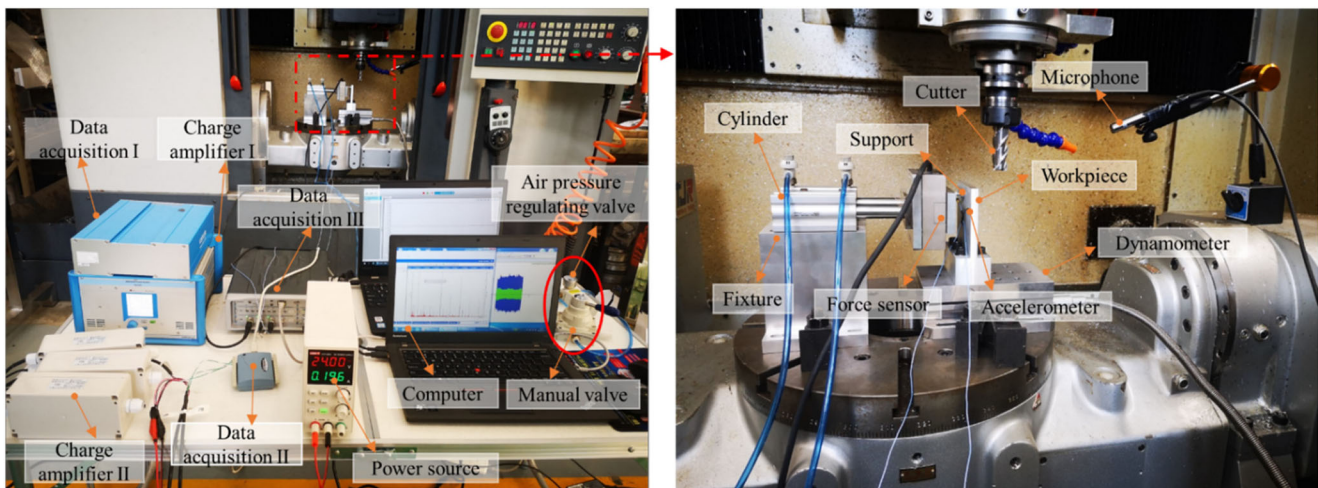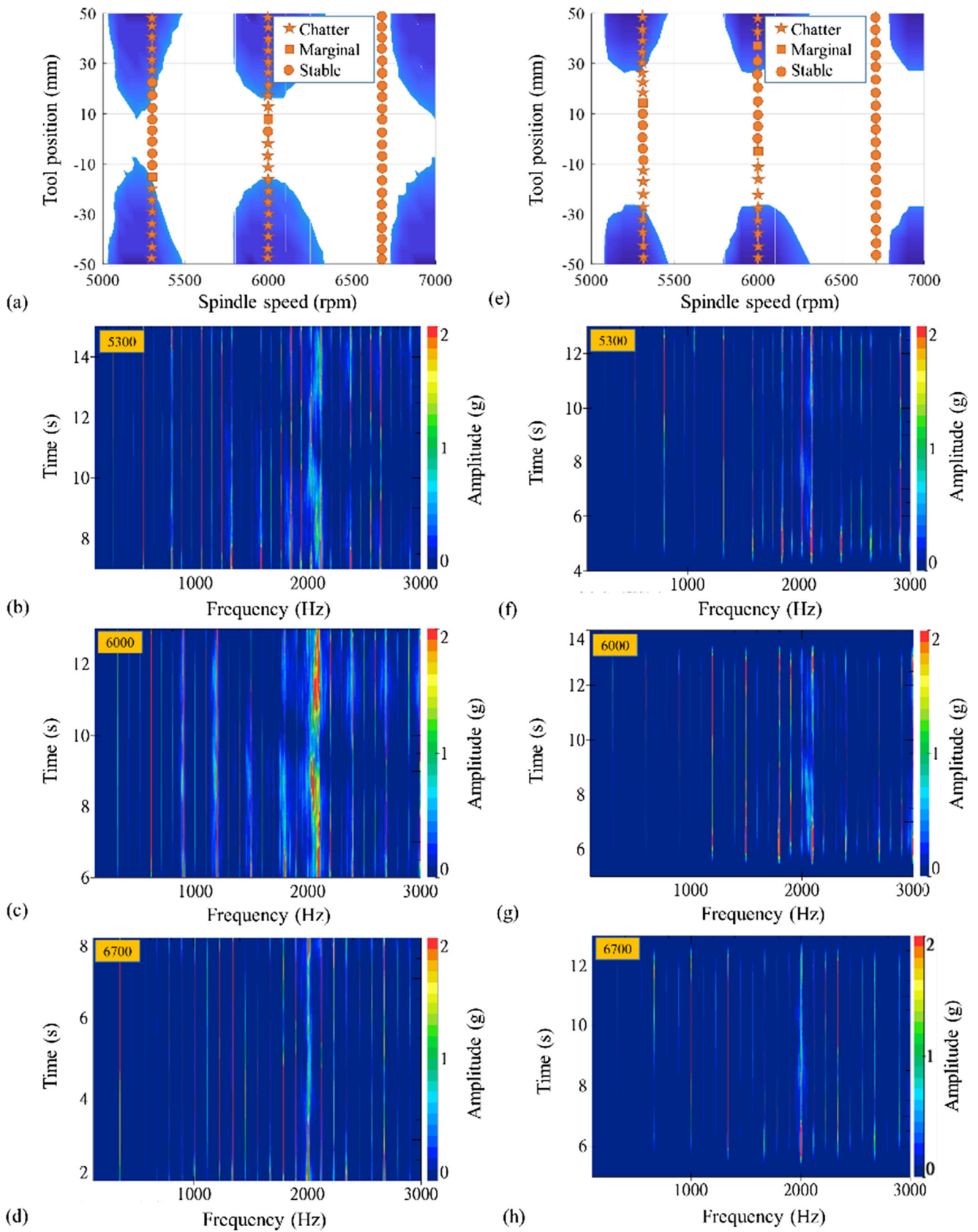

Fig. 9 Experimental setup

Fig. 10 SLDs and time-frequency diagrams. **a–d** Without support. **e–h** With support

depth of cut is $a_r = 0.2mm$ and the feed rate is $f_t = 0.05mm/$ tooth. Three spindle speeds are selected to validate the prediction results: $\Omega = 5300rpm$, 6000rpm, and 6700rpm. The cutting status is judged by means of short-time Fourier transform (STFT) on acceleration signals. Chatter, marginal, and stable conditions are labeled using pentagram, square, and circle markers, respectively.

STFT diagrams for cases without fixture support are shown in Fig. 10 b–d. When the spindle speed is 5300rpm, the chatter energy is obvious around 2000Hz at the beginning and end of tool path while negligible at the middle. When the spindle speed is 6000rpm, the frequency spectra are similar to those of 5300rpm, but the chatter energy is more obvious around 2000Hz. In addition, chatter frequencies also appear near 1000Hz. When the speed is 6700rpm, there is no obvious chatter energy on the whole path. It validates that the theoretical stability prediction results are in good agreement with the cutting tests for cases without fixture support.
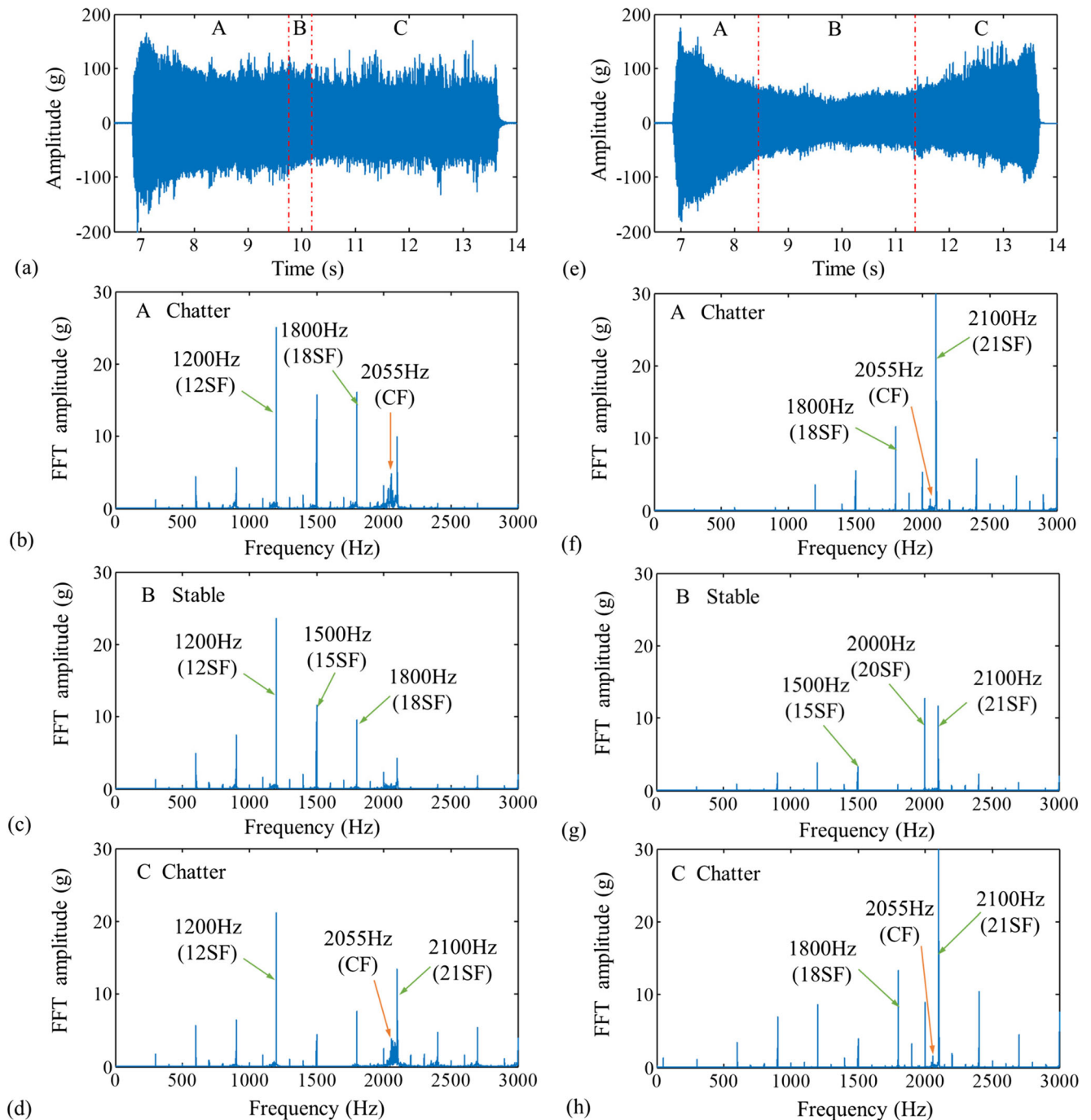

Fig. 11 Acceleration signals and frequency spectra for 6000rpm. **a–d** Without support. **e–h** With support
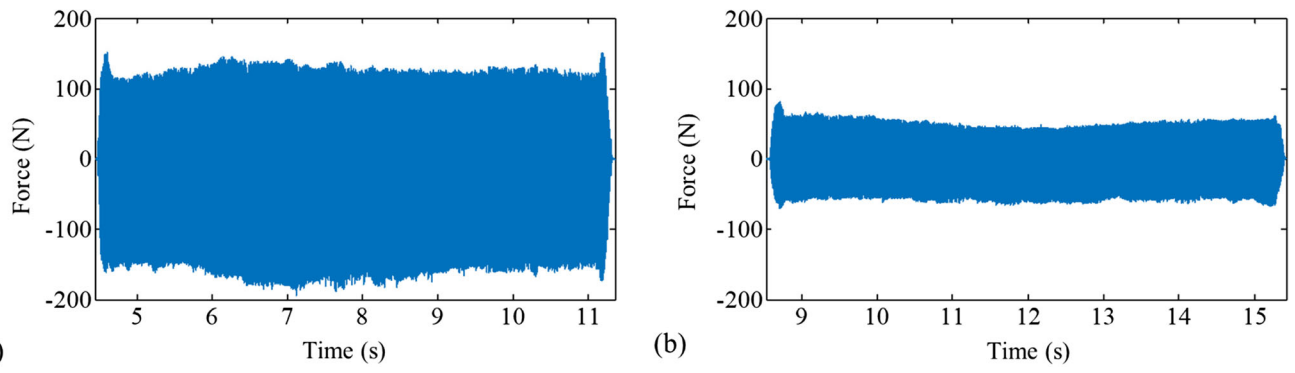
Fig. 12 Cutting force signals of workpiece. **a** Without support. **b** With support
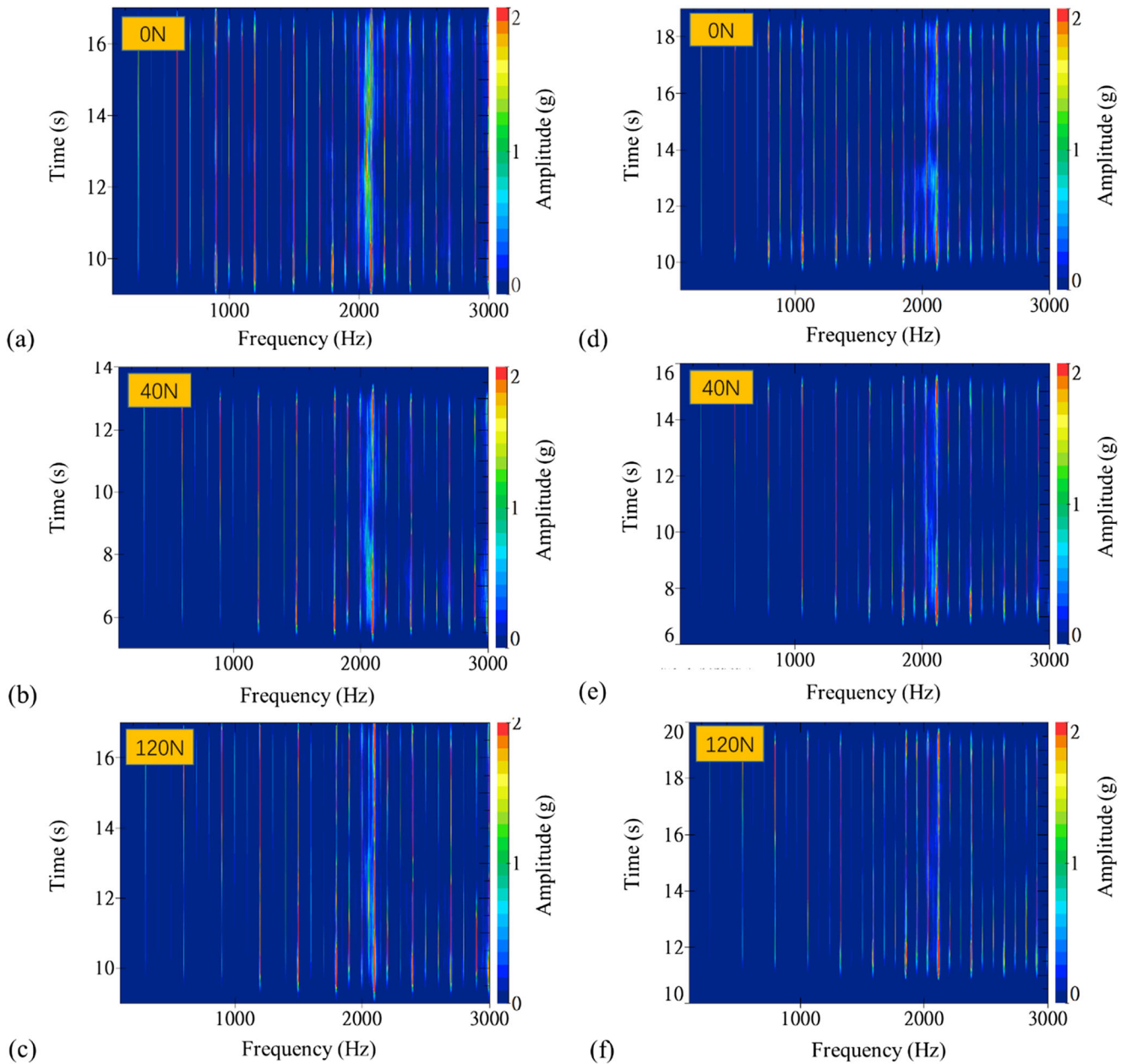

Fig. 13 Time-frequency diagrams of acceleration signals under different supporting conditions: **a–c** 6000rpm. **d–f** 5300rpm

STFT diagrams for cases with fixture support are shown in Fig. 10 f–h. Similarly, experimental results reveal that chatter happens at the beginning and end of tool path for 5300rpm and 6000rpm. It is stable on the whole path for 6700rpm. It indicates that the proposed method can successfully predict the stability for thin-walled workpieces with fixture support. The slight discrepancies may attribute to the reason that the introduction of support makes the theoretical model more complicated, which deserves further exploration.

In addition, STFT diagrams also reveal that fixture support can remarkably mitigate the chatter energy, even if it cannot completely prevent the occurrence of chatter, as shown in Fig. 10 b versus f and c versus g. Take 6000rpm as an example. The cutting acceleration signals are compared in detail from the viewpoint of time-history evolution and frequency spectra.

As shown in Fig. 11 a and e, in general, the amplitude of acceleration for case with fixture support is smaller than that for case without fixture support, especially at the middle of tool path. Besides, the envelope of time domain signals for case with fixture support also appears smoother. Through dividing the cutting signals into three parts, the frequency spectra are obtained by performing fast Fourier transform (FFT), as shown in Fig. 11 b–d and f–h, where the symbol "SF" stands for "spindle rotation frequency" and "CF" stands for "Chatter frequency". FFT diagrams validate the stability prediction results again: chatter happens at the beginning and end of tool path, while stable cutting locates at the middle. In addition, the length of stable cutting signals labeled B in Fig. 11 e is larger than the counterpart in Fig. 11 a. It reveals that the utilization of fixture support expands the stable zone of thin-walled workpiece.

To further validate the effect of fixture support on stability improvement, the measured cutting force signals in thickness direction are also compared in time domain, as shown in Fig. 12. The amplitude of cutting forces after utilization of fixture support decreases by about 60%.

4.2 Cutting tests under different support forces

In this section, the influence of support forces on milling dynamics of thin-walled workpiece is further explored. Five supporting conditions are selected: without support, 0N, 40N, 80N, and 120N. It is worth noting that there is essential distinction between the case without support and the case with 0N support force. "Without support" means the fixture is out of contact with the thin-walled workpiece. "0N" means the fixture is in contact with the workpiece but the support force is 0N. For 0N conditions, there exist complicated interactions when the workpiece vibrates under cutting excitation.

Cutting tests under different supporting conditions are carried out for the spindle speed 6000rpm and 5300rpm, respectively. Similarly, acceleration signals are selected for STFT analysis, as shown in Fig. 13. Since the cases without support

and 80N have been analyzed in Section 4.1, only the rest supporting conditions are displayed.

The results show that fixture support can effectively mitigate the chatter energy in milling process of thin-walled workpiece. Even for 0N case, the chatter energy in Fig. 13 a also decreases a lot in comparison with the case without support in Fig. 10 c. Generally speaking, the chatter mitigation performance of fixture improves with the increase of support force. But when the support force reaches certain value, the performance improvement becomes minimal and negligible. For example, the time-frequency diagram for 80N is similar with that for 120N, as shown in Fig. 10 g versus Fig. 13 c for 6000rpm and Fig. 10 f versus Fig. 13 f for 5300rpm.

The above phenomenon is consistent with the influence of support forces on FRF in Fig. 5. It is attributed to the complicated contact status between fixture and workpiece. Prior to stable contact, the vibration mitigation performance of fixture increases with the growth of support forces. But when a stable contact is established with enough preloading, the effectiveness of support force becomes saturated.

5 Conclusion and discussion

In this paper, the influence of fixture support force on milling dynamics of thin-walled workpiece is systematically investigated on the basis of designed force-tunable pneumatic fixture. Cutting experiments validate the built dynamic model of tool-workpiece-fixture system and the predicted 3D stability lobe diagrams. Detailed analyses on FRF change, stability improvement, and cutting signals under different fixture supporting conditions draw some important conclusions:

(1) Fixture can significantly shift the natural frequency of thin-walled workpiece and reduce the FRF amplitude of target mode.

(2) In general, fixture expands the chatter-free zone of thin-walled workpiece. Even for chatter conditions, fixture can significantly mitigate the chatter frequency energy.

(3) The influence of fixture supporting force on stability limits and cutting signals is closely related to the contact status between fixture and workpiece. The cutting performance can be enhanced by increasing the supporting force, but there exists a critical value, beyond which the improvement will become saturated.

The basic rules of fixture supporting forces on milling dynamics of thin-walled workpieces are explored in this paper. Nevertheless, the interaction mechanism between fixture and workpiece during machining process remains to be investigated further in the future.

Data availability Data will be available upon request.

Code availability The commercial ABAQUS code was used for the numerical model.

Declarations

Ethical approval This work does not contain any studies with human participants or animals performed by any of the authors.

Consent to participate Not applicable.

Consent to publish All authors have read and agreed to the published version of the manuscript.

Conflict of interest The authors declare no competing interests.

References

1. Munoa J, Beudaert X, Dombovari Z, Altintas Y, Budak E, Brecher C, Stepan G (2016) Chatter suppression techniques in metal cutting. CIRP Ann-Manuf Technol 65(2):785–808. https://doi.org/10.1016/j.cirp.2016.06.004

2. Niu JB, Xu JT, Ren F, Sun YW, Guo DM (2021) A short review on milling dynamics in low-stiffness cutting conditions: modeling and analysis. J Adv Manuf Sci Technol 1:2020004–2020000. https://doi.org/10.51393/j.jamst.2020004

3. Yuwen, SUN Jinjie, JIA Jinting, XU Mansen, CHEN Jinbo, NIU (2021) Path feedrate and trajectory planning for free-from surface machining: A state-of-the-art review. Chinese J Aeronaut. https://doi.org/10.1016/j.cja.2021.06.011

4. Niu JB, Jia JJ, Sun YW, Guo DM (2020) Generation mechanism and quality of milling surface profile for variable pitch tools considering runout. J Manuf Sci Eng 142(12):121001. https://doi.org/10.1115/1.4047622

5. Altintas Y (2012) Manufacturing automation: metal cutting mechanics, machine tool vibrations, and CNC design. Cambridge University Press

6. Altintas Y, Budak E (1995) Analytical prediction of stability lobes in milling. CIRP Ann-Manuf Technol 44(1):357–362. https://doi.org/10.1016/S0007-8506(07)62342-7

7. Merdol SD, Altintas Y (2004) Multi frequency solution of chatter stability for low immersion milling. J Manuf Sci Eng 126(3):459–466. https://doi.org/10.1115/1.1765139

8. Insperger T, Stepan G (2004) Updated semi-discretization method for periodic delay-differential equations with discrete delay. Int J Numer Methods Eng 61(1):117–141. https://doi.org/10.1002/nme.1061

9. Ding Y, Zhu LM, Zhang XJ, Ding H (2010) A full-discretization method for prediction of milling stability. Int J Mach Tools Manuf 50(5):502–509. https://doi.org/10.1016/j.ijmachtools.2010.01.003

10. Bravo U, Altuzarra O, López de Lacalle LN, Sánchez JA, Campa FJ (2005) Stability limits of milling considering the flexibility of the workpiece and the machine. Int J Mach Tools Manuf 45(15):1669–1680. https://doi.org/10.1016/j.ijmachtools.2005.03.004

11. Budak E, Tunç LT, Alan S, Özgüven HN (2012) Prediction of workpiece dynamics and its effects on chatter stability in milling. CIRP Ann-Manuf Technol 61(1):339–342. https://doi.org/10.1016/j.cirp.2012.03.144

12. Song QH, Liu ZQ, Wan Y, Ju GG, Shi JH (2015) Application of Sherman-Morrison-Woodbury formulas in instantaneous dynamic of peripheral milling for thin-walled component. Int J Mech Sci 96-97:79–90. https://doi.org/10.1016/j.ijmecsci.2015.03.021

13. Eksioglu C, Kilic ZM, Altintas Y (2012) Discrete-time prediction of chatter stability, cutting forces, and surface location errors in flexible milling systems. J Manuf Sci Eng 134(6):0610066. https://doi.org/10.1115/1.4007622

14. Sun YW, Jiang SL (2018) Predictive modeling of chatter stability considering force-induced deformation effect in milling thin-walled parts. Int J Mach Tool Manu 135:38–52. https://doi.org/10.1016/j.ijmachtools.2018.08.003

15. Adetoro OB, Sim WM, Wen PH (2010) An improved prediction of stability lobes using nonlinear thin wall dynamics. J Mater Process Technol 210(6-7):969–979. https://doi.org/10.1016/j.jmatprotec.2010.02.009

16. Jin X, Sun YW, Guo Q, Guo DM (2016) 3D stability lobe considering the helix angle effect in thin-wall milling. J Adv Manuf Technol 82(9-12):2123–2136. https://doi.org/10.1007/s00170-015-7570-8

17. Yulei, Ji Qingzhen, Bi Shaokun, Zhang Yuhan, Wang (2018) A new receptance coupling substructure analysis methodology to predict tool tip dynamics. Int J Mach Tools Manuf:12618–12626. https://doi.org/10.1016/j.ijmachtools.2017.12.002

18. Schmitz TL, Couey J, Marsh E, Mauntler N, Hughes D (2007) Runout effects in milling: surface finish, surface location error, and stability. Int J Mach Tool Manu 47(5):841–851. https://doi.org/10.1016/j.ijmachtools.2006.06.014

19. Zhang XJ, Xiong CH, Ding Y, Feng MJ, Xiong YL (2012) Milling stability analysis with simultaneously considering the structural mode coupling effect and regenerative effect. Int J Mach Tool Manu 53(1):127–140. https://doi.org/10.1016/j.ijmachtools.2011.10.004

20. Zhang Z, Luo M, Wu BH, Zhang DH (2020) Dynamic modeling and stability prediction in milling process of thin-walled workpiece with multiple structural modes. Proc IMechE Part B: J Eng Manuf:1–14. https://doi.org/10.1177/0954405420933710

21. Niu JB, Jia JJ, Wang RQ, Xu JT, Sun YW, Guo DM (2021) State dependent regenerative stability and surface location error in peripheral milling of thin-walled parts. Int J Mech Sci 196:106294. https://doi.org/10.1016/j.ijmecsci.2021.106294

22. Kolluru K, Axinte D (2014) Novel ancillary device for minimising machining vibrations in thin wall assemblies. Int J Mach Tool Manu 85:79–86. https://doi.org/10.1016/j.ijmachtools.2014.05.007

23. Ma JJ, Zhang DH, Wu BH, Luo M, Liu YL (2017) Stability improvement and vibration suppression of the thin-walled workpiece in milling process via magnetorheological fluid flexible fixture. J Adv Manuf Technol 88(5-8):1231–1242. https://doi.org/10.1007/s00170-016-8833-8

24. Fei JX, Lin B, Xiao JL, Ding M, Yan S, Zhang XF, Zhang J (2018) Investigation of moving fixture on deformation suppression during milling process of thin-walled structures. J Manuf Process 32:403–411. https://doi.org/10.1016/j.jmapro.2018.03.011

25. Meshreki M, Attia H, Koevecses J (2011) A new analytical formulation for the dynamics of multipocket thin-walled structures considering the fixture constraints. J Manuf Sci Eng 133(2):021014. https://doi.org/10.1115/1.4003520

26. Meshreki M, Attia H, Koevecses J (2011) Development of a new model for the varying dynamics of flexible pocket-structures during machining. J Manuf Sci Eng 133(4):041002. https://doi.org/10.1115/1.4004322

27. Wan XJ, Zhang Y (2013) A novel approach to fixture layout optimization on maximizing dynamic machinability. Int J Mach Tool Manu 70:32–44. https://doi.org/10.1016/j.ijmachtools.2013.03.007

28. Wan XJ, Zhang Y, Huang XD (2013) Investigation of influence of fixture layout on dynamic response of thin-wall multi-framed workpiece in machining. Int J Mach Tool Manu 75:87–99. https://doi.org/10.1016/j.ijmachtools.2013.09.008

29. Qin G, Zhang W, Wu Z, Wan M (2007) Systematic modeling of workpiece-fixture geometric default and compliance for the prediction of workpiece machining error. J Manuf Sci Eng 129(4):789–801. https://doi.org/10.1115/1.2336260

30. Wan XJ, Xiong CH, Wang XF, Zhang XM, Xiong YL (2009) Analysis–synthesis of dimensional deviation of the machining feature for discrete-part manufacturing processes. Int J Mach Tool Manu 49(15):1214–1233. https://doi.org/10.1016/j.ijmachtools.2009.07.014

31. Marin RA, Ferreira PM (2003) Analysis of the influence of fixture locator errors on the compliance of work part features to geometric tolerance specifications. J Manuf Sci Eng 125(3):609–616. https://doi.org/10.1115/1.1578669

32. Liu SG, Zheng L, Zhang ZH, Li ZZ, Liu DC (2007) Optimization of the number and positions of fixture locators in the peripheral milling of a low-rigidity workpiece. J Adv Manuf Technol 33(7-8):668–676. https://doi.org/10.1007/s00170-006-0507-5

33. Raghu A, Melkote SN (2004) Analysis of the effects of fixture clamping sequence on part location errors. Int J Mach Tool Manu 44(4):373–382. https://doi.org/10.1016/j.ijmachtools.2003.10.015

34. Siebenaler SP, Melkote SN (2006) Prediction of workpiece deformation in a fixture system using the finite element method. Int J Mach Tool Manu 46(1):51–58. https://doi.org/10.1016/j.ijmachtools.2005.04.007

35. Matsubara A, Taniyama Y, Wang J, Kono D (2017) Design of a support system with a pivot mechanism for suppressing vibrations in thin-wall milling. CIRP Ann Manuf Technol 66(1):381–384. https://doi.org/10.1016/j.cirp.2017.04.055

36. Zhong WP, Hu SJ (2006) Modeling machining geometric variation in a N-2-1 fixturing scheme. J Manuf Sci Eng 128(1):213–219. https://doi.org/10.1115/1.2114927

37. Hao XZ, Li YG, Chen GX, Liu CQ (2018) 6+X locating principle based on dynamic mass centers of structural parts machined by responsive fixtures. Int J Mach Tool Manu 125:112–122. https://doi.org/10.1016/j.ijmachtools.2017.11.006

38. Hao XZ, Li YG, Zhao ZW, Liu CQ (2019) Dynamic machining process planning incorporating in-process workpiece deformation data for large-size aircraft structural parts. Int J Comput Integr Manuf 32(2):136–147. https://doi.org/10.1080/0951192X.2018.1529431

39. Jiang SL, Sun YW (2020) Stability analysis for a milling system considering multi-point-contact cross-axis mode coupling and cutter run-out effects. Mech Syst Signal Process 141:106452. https://doi.org/10.1016/j.ymssp.2019.106452

40. Niu JB, Ding Y, Zhu LM, Ding H (2017) Mechanics and multi-regenerative stability of variable pitch and variable helix milling tools considering runout. Int J Mach Tool Manu 123:129–145. https://doi.org/10.1016/j.ijmachtools.2017.08.006

41. Jiang SL, Sun YW (2018) A multi-order method for predicting stability of a multi-delay milling system considering helix angle and run-out effects. Chin J Aeronaut 31(6):1375–1387. https://doi.org/10.1016/j.cja.2017.08.005

42. Wan M, Zhang WH (2009) Systematic study on cutting force modelling methods for peripheral milling. Int J Mach Tool Manu 49(5):424–432. https://doi.org/10.1016/j.ijmachtools.2008.12.004